

# First-order kinetics bottleneck during photoinduced ultrafast insulator-metal transition in 3D orbitally-driven Peierls insulator $\text{CuIr}_2\text{S}_4$

M. Naseska<sup>1</sup>, P. Sutar<sup>1</sup>, Y. Vaskivskiy<sup>1</sup>, I. Vaskivskiy<sup>1</sup>, D. Vengust<sup>1</sup>,  
D. Svetin<sup>1</sup>, V. V. Kabanov<sup>1</sup>, D. Mihailovic<sup>1,2</sup>, T. Mertelj<sup>1,2</sup>

<sup>1</sup>*Complex Matter Department, Jozef Stefan Institute, Jamova 39, 1000 Ljubljana, Slovenia and*  
<sup>2</sup>*Center of Excellence on Nanoscience and Nanotechnology Nanocenter*  
(CENN Nanocenter), Jamova 39, 1000 Ljubljana, Slovenia\*

The spinel-structure  $\text{CuIr}_2\text{S}_4$  compound displays a rather unusual orbitally-driven three-dimensional Peierls-like insulator-metal transition. The low- $T$  symmetry-broken insulating state is especially interesting due to the existence of a metastable irradiation-induced disordered weakly conducting state. Here we study intense femtosecond optical pulse irradiation effects by means of the all-optical ultrafast multi-pulse time-resolved spectroscopy. We show that the structural coherence of the low- $T$  broken symmetry state is strongly suppressed on a sub-picosecond timescale above a threshold excitation fluence resulting in a structurally inhomogeneous transient state which persists for several-tens of picoseconds before reverting to the low- $T$  disordered weakly conducting state. The electronic order shows a transient gap filling at a significantly lower fluence threshold. The data suggest that the photoinduced-transition dynamics to the high- $T$  metallic phase is governed by first-order-transition nucleation kinetics that prevents the complete ultrafast structural transition even when the absorbed energy significantly exceeds the equilibrium enthalpy difference to the high- $T$  metallic phase. In contrast, the dynamically-decoupled electronic order is transiently suppressed on a sub-picosecond timescale rather independently due to a photoinduced Mott transition.

*Keywords:* ultrafast metal-insulator transition, ultrafast optical spectroscopy, transient reflectivity, coherent phonons,  $\text{CuIr}_2\text{S}_4$ , spinel

## I. INTRODUCTION

Kinetics of first order phase transitions are important both from the point of view of applications as well as fundamental science. For example, the control of kinetics during the transformation of various forms of steel<sup>1</sup> is used to tailor its microstructural and mechanical properties. An example of interesting fundamental physics related to first order phase transition kinetics is inflation of the early universe, where a supercooled metastable system might have been transformed via droplet nucleation into the Higgs-field broken-symmetry state<sup>2</sup>.

In solids, ultrafast first-order insulator-metal (IM) phase transitions could be instrumental for ultrafast sensor and nonvolatile memory applications. Their ultrafast kinetics therefore attracted a great deal of attention<sup>3–26</sup> with strong focus on  $\text{VO}_2$ <sup>3,5,7,8,12,13,15,19,24–26</sup>,  $\text{V}_2\text{O}_3$ <sup>14,18,21,23</sup> and  $1T\text{-TaS}_2$ <sup>6,11,16,20,22</sup>. There are however still open questions how the inherent first-order meta-stability manifests itself when phases with concurrent electronic and lattice orders are driven across the first-order phase boundary on ultrafast time scales.

In  $\text{VO}_2$ , for example, the change of the low- $T$  electronic-order-induced monoclinic lattice potential is believed to be rather abrupt<sup>7,8,19,24</sup> with a sub-picosecond V-V dimerization suppression suggesting that the high- $T$  metallic rutile phase symmetry is restored on a  $\sim 100$ -fs timescale. This is contrasted by recent observation of an additional transient metastable monoclinic metallic phase in a significant fraction of the

polycrystalline sample grains<sup>25</sup>. While the presence of the metastable monoclinic metallic phase is still rather controversial<sup>26</sup> the electronic and lattice orders might be transiently decoupled with the emergence of the metallic rutile lattice structure somehow inhibited.

In  $\text{V}_2\text{O}_3$  the inherent first-order meta stability plays a determining role with the nucleation and growth kinetics of the metallic nanodroplets governing the dynamics across the first-order IM phase transition<sup>14,23</sup>. The importance of the nucleation and growth kinetics was noted also in a first-order ultrafast charge-density-wave phase transformation in  $1T\text{-TaS}_2$ <sup>16,20</sup>.

An interesting opportunity for studying the ultrafast first-order IM phase transition<sup>30</sup> kinetics is offered in the spinel-structure  $\text{CuIr}_2\text{S}_4$  compound that shows a rather unusual orbitally-driven<sup>28</sup> three-dimensional Peierls-like IM transition. Upon cooling, the metallic cubic (MC) phase (Figure 1 (a)) undergoes a first order transition to a triclinic<sup>31,32</sup> insulating phase (Figure 1 (b)) at  $T_{\text{IM}} \sim 233$  K. The triclinic insulating phase is characterized by  $\text{Ir}^{3+}:\text{Ir}^{4+}$  charge disproportionation accompanied with Peierls-like dimerization of  $\text{Ir}^{4+}$ -ion pairs along a set of cubic  $\langle 110 \rangle$  and  $\langle -110 \rangle$  Ir-ion rows alternating along the corresponding  $\langle 001 \rangle$  direction.

The transition can be understood in terms of quasi-1D  $\text{Ir-}t_{2g}$ -orbitals derived hybridized bands that are split due to the band Jahn-Teller effect into two narrower fully occupied  $xz$ - and  $yz$ -derived bands and a broader  $3/4$  occupied  $xy$ -derived band that simultaneously becomes gaped due to the Peierls tetramerization (see Fig 1 (c))<sup>28</sup>. The  $\text{Ir-}5d$  orbitals appear broad enough that the correlation effects do not play a major role in the transition<sup>28,29,33</sup> contrary to  $\text{V}_2\text{O}_3$  and  $\text{VO}_2$ .

The  $\text{CuIr}_2\text{S}_4$  is interesting also due to the low temperature X-ray- and visible-light-induced metastable disor-

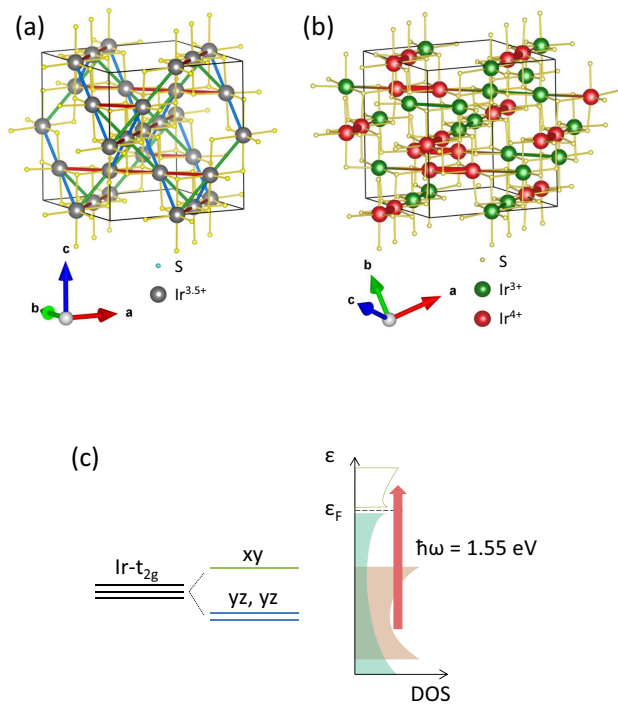


Figure 1.  $\text{CuIr}_2\text{S}_4$  structure. (a) Schematics<sup>27</sup> of the  $\text{CuIr}_2\text{S}_4$  structure in the high- $T$  metallic phase. The different sets of Ir-ion rows alternating along the  $\langle 110 \rangle$  or  $\langle -110 \rangle$  cubic directions are indicated by the differently colored bonds. (b) In the low- $T$  insulating phase one set of rows undergoes a Peierls distortion with the  $\text{Ir}^{4+}$  dimers (red dumbbells) interleaved with  $\text{Ir}^{3+}$ -ion pairs (green). The compasses indicate the basis orientations while the black lines indicate the high- $T$  cubic unit cell. The Cu ions are omitted for clarity. (c) A schematic diagram of the  $\text{Ir}-t_{2g}$ -orbitals derived quasi-1D electronic bands density of states in the low- $T$  phase<sup>28</sup>. The shaded regions correspond to the occupied states and the dominant optical transitions at the experimental photon energy<sup>29</sup> are indicated by the red arrow.

dered weakly conducting (DWC) phase<sup>34–39</sup>. The presence of short-range incommensurate structural correlations observed<sup>37</sup> in the DWC phase suggests presence of *competing instabilities* that appear after suppression of the insulating phase. The formation of the DWC phase was studied mostly with weak continuous excitations. Competing instabilities, however, might lead to formation of even more conducting metastable state under strongly nonequilibrium conditions as in the case of  $1T$ - $\text{TaS}_2$ , where a strong ultrafast excitation leads to a metastable hidden (H) metallic phase<sup>11</sup>. In order to search for a possible hidden metallic state, different from the DWC phase, and to study kinetics during ultrafast first-order IM phase transition in  $\text{CuIr}_2\text{S}_4$  we therefore performed a systematic femtosecond multi-pulse all-

optical investigation of the single-crystal transient reflectivity relaxation dynamics in  $\text{CuIr}_2\text{S}_4$  as a function of excitation fluence.

The low- $T$  quasi-equilibrium transient reflectivity in  $\text{CuIr}_2\text{S}_4$  is dominated by the low-frequency broken-symmetry-induced coherent-phonons response that discontinuously vanishes across the equilibrium IM transition.<sup>40</sup> The coherent response can therefore be used as a time-resolved probe for the broken-lattice-symmetry dynamics in the strongly excited low- $T$  phases.<sup>8,41</sup> This can be done by means of our advanced multi-pulse method<sup>41</sup>, where we use a strong driving laser pulse to *initiate* a photoinduced transition and *probe* the subsequent evolution by means of a weaker pump- (P) probe (Pr) pulses sequence.

## II. METHODS

### Sample growth and characterization

Single crystals of  $\text{CuIr}_2\text{S}_4$  were grown from Bi solution and characterized as described in Ref.<sup>40</sup>. Here we present ultrafast optical data from two cleaved crystals designated S1 and S2. The orientation of the S1 cleaved surface was determined from electron back scatter diffraction Kikuchi patterns to be close to the  $\langle 221 \rangle$  plane while the orientation of the S2 cleaved surface was inferred from the Raman selection rules to be close to the  $\langle 001 \rangle$  plane.<sup>40</sup>

### Multi-pulse transient reflectivity measurements

The multi-pulse transient reflectivity measurements<sup>41,42</sup> were performed using 50-fs linearly polarized laser pulses at 800 nm wavelength and the 200 – 250 kHz repetition rate. In addition to the pump (P) and probe (Pr) pulses at  $\hbar\omega = 1.55$  eV we used another intense driving (D) pulse (also at  $\hbar\omega = 1.55$  eV) with a variable delay with respect to the pump (P) pulse (see Figure 2).

The multi-pulse transient reflectivity  $\Delta R_3/R$  was measured by monitoring the intensity of the Pr beam. The direct contribution of the unchopped D beam to the total transient reflectivity,  $\Delta R$ , was rejected by means of a lock-in synchronized to the chopper that modulated the intensity of the P beam only. Due to the chopping scheme the measured quantity in the multi-pulse experiments is the difference between the transient reflectivity in the presence of P and D pulses,  $\Delta R_{\text{DP}}(t_{\text{Pr}}, t_{\text{P}}, t_{\text{D}})$ , and the transient reflectivity in the presence of the D pulse only,  $\Delta R_{\text{D}}(t_{\text{Pr}}, t_{\text{D}})$ :

$$\Delta R_3(t_{\text{Pr}}, t_{\text{P}}, t_{\text{D}}) = \Delta R_{\text{DP}}(t_{\text{Pr}}, t_{\text{P}}, t_{\text{D}}) - \Delta R_{\text{D}}(t_{\text{Pr}}, t_{\text{D}}), \quad (1)$$

where  $t_{\text{Pr}}$ ,  $t_{\text{P}}$  and  $t_{\text{D}}$  correspond to the Pr, P and D pulse arrival times, respectively. In the limit of vanishing D

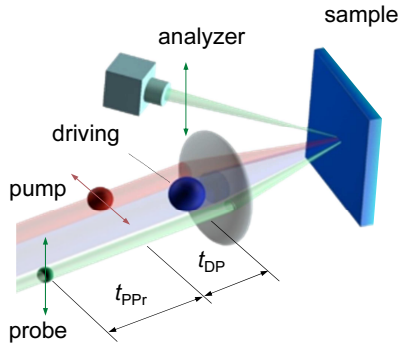


Figure 2. Schematics of the multi-pulse experiment with notation of the delays adapted from Ref.<sup>43</sup>.

pulse fluence  $\Delta R_3/R$  reduces to the standard two-pulse transient reflectivity  $\Delta R/R$ .

The P/D and Pr beam diameters were in the ranges of 40-70 and 18-30  $\mu\text{m}$ , respectively. The probe fluence was  $\sim 50 \mu\text{J}/\text{cm}^2$ . For the multi-pulse measurements the fluence of the P pulse,  $\mathcal{F}_P \lesssim 100 \mu\text{J}/\text{cm}^2$ , was kept in the linear response region. The polarizations of the P and D beams were perpendicular to the probe beam polarization with a random orientation with respect to the crystal axes.

### III. RESULTS

The DWC phase emergence depends on the absorbed dose<sup>35,44</sup>, but the threshold dose was determined only for the case of high-energy ion irradiation<sup>44</sup>. Since the exact optical DWC-phase-creation conditions are not known we measured also the low- $T$  DC photoconductivity (see Supplemental Material (SM)<sup>45</sup>) and found, as suggested previously,<sup>40</sup> that even at the lowest feasible excitation fluences,  $F \sim 100 \mu\text{J}/\text{cm}^2$ , the threshold dose is exceeded on a timescale faster than a single transient reflectivity scan acquisition time of  $\sim 100$  s. The pristine insulating triclinic phase is therefore inaccessible in the pump-probe experiments at low  $T$  and the previously reported<sup>40</sup> equilibrium low- $T$  transient reflectivity refers to the DWC phase. Despite the absence of a long range  $\text{Ir}^{4+}$ -dimer order in the DWC phase<sup>37</sup> the previously characterized coherent oscillations (CO) due to the dispersive excitation of coherent phonons<sup>40,45,46</sup> (DECP) show well defined peaks with the low- $T$  dephasing times exceeding  $\sim 100$  ps.

In Figure 3 (a) we show the pump fluence,  $F_P$ , dependence of the standard two-pulse transient reflectivity,  $\Delta R/R$ , at  $T = 9$  K. The CO scale almost linearly with increasing  $F_P$  up to  $\sim 2 \text{ mJ}/\text{cm}^2$ . With increasing  $F_P$  the CO appear suppressed in the  $F_P$ -normalized scans and the signal becomes dominated by the sub-ps relaxation component. The detailed DECP-model<sup>40,45</sup>

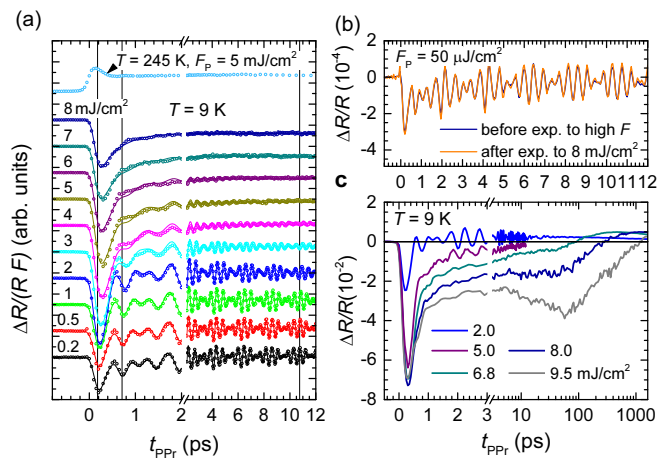


Figure 3. Transient reflectivity pump-fluence dependence. (a) Fluence-normalized transient reflectivity as a function of  $F_P$  in the low- $T$  phase. A high- $T$  MC-phase trace ( $T = 245$  K) is shown on top for comparison. Due to the normalization the absence of changes at low  $F_P$  indicates linear scaling with  $F_P$ . The traces are vertically offset for clarity and the thin lines correspond to the DECP model fit. (b) The low- $F_P$  transient reflectivity before and after exposure at the highest  $F_P$ . (c) Transient reflectivity at elevated  $F_P$  at longer delay. Please note the logarithmic scale after the break.

component analysis (see. Figure 4) reveals that the sub-ps exponential component (SEC) amplitude,  $A_e$ , departs from the low- $F_P$  linear dependence and starts to increase more steeply above  $F_{ce} \sim 0.6 \text{ mJ}/\text{cm}^2$  already (see inset to Figure 4 (e)). Concurrently, the amplitudes of the three weaker, high-frequency modes, designated O3, O4 and O5, show an onset of saturation while the amplitudes of the two stronger, low-frequency modes, O1 and O2, show an increased slope. Above  $F_c \sim 3 \text{ mJ}/\text{cm}^2$  the amplitudes of all modes drop and vanish at the highest  $F_P$ . The SEC does not show any anomalies around  $F_c$ , but shows saturation of  $A_e$  and the relaxation time,  $\tau_e$ , above  $F_P \sim 5 \text{ mJ}/\text{cm}^2$ .

The high- $F$  transient reflectivity shows an initial fast,  $\tau_e = 0.5$  ps, relaxation followed by slower  $F$ -dependent dynamics (see Figure 3 (c)). The slow dynamics sets in above  $F_P \sim 5 \text{ mJ}$  and consists of a plateau emerging into a broad dip at  $\sim 60$  ps at the highest  $F_P$  followed by relaxation extending to a  $\sim 1$  ns timescale.

The high- $F_P$  slow dynamics was investigated further by means of the multi-pulse experiments. The multi-pulse transient reflectivity,  $\Delta R_3/R$ , well above  $F_c$  is shown in Figure 5 for different D-P delays,  $t_{DP}$ . At short  $t_{DP}$ , the multi-pulse transient reflectivity resembles the 2-pulse transient reflectivity of the low- $T$  state around  $F_P \sim F_c$ , but, with *much strongly damped* CO. After  $t_{DP} \sim 5$  ps the CO start to gradually reemerge also on longer P-Pr delays,  $t_{PPp}$ . The multipulse transients are *completely different* from the high- $T$  MC phase transients indicating that the highly excited transient state cannot be associated with the high- $T$  MC phase.

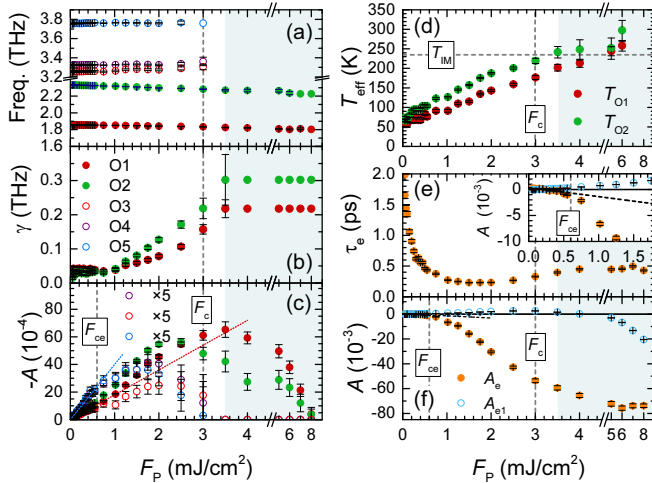


Figure 4. Pump fluence dependence of the DECP fit parameters. (a) The frequency, (b) damping and (c) amplitude of the coherent oscillations as a function of  $F_P$ . In the shaded region, above  $F_P \sim 3.5$  mJ/cm<sup>2</sup>, the coherent oscillations cannot be completely described by the DECP theory. (d) The effective temperature (see text) obtained from the frequency shifts of the two strongest coherent modes as a function of  $F_P$ . (e) The relaxation time and (f) amplitude of the exponential components as a function of  $F_P$ . The black dashed line is the extrapolation of the low  $F_P$  behavior. The inset to (e) shows (f) in expanded scale. The vertical and horizontal dashed lines in correspond to  $F_{ce}$ ,  $F_c$  and  $T_{IM}$ , respectively.

The DECP fit component analysis shown in Figure 6 indicates that the initial amplitudes of the strongest two modes (see Figure 6 (c)) *do not appear suppressed* even immediately after the D pulse while the damping factors (see Figure 6 (b)) exceed the equilibrium value<sup>40</sup> of  $\sim 0.01$  THz by up to two orders of magnitude recovering by an order of magnitude on a  $\sim 100$  ps  $t_{DP}$  timescale. Just before the arrival of the subsequent D pulse, after 5  $\mu$ s, the damping is reduced close to the equilibrium-state value, together with exponential components parameters (Figure 6 (e) and (f)). The low- $T$  state is therefore completely recovered after each D pulse, albeit, at a higher  $T$  than the cryostat base temperature due to the heat buildup. The behavior is similar also at an increased  $F_D = 8.1$  mJ/cm<sup>2</sup> with slower recovery.<sup>45</sup>

The suppression of the CO is delayed with respect to the D pulse for  $\sim 0.6$  ps (see inset to Figure 5) and does not depend on the small changes of the  $t_{DP}$  delay<sup>45</sup>. The delay is consistent with the duration of the initial sub-picosecond transient observed for the high- $F$  transient reflectivity in Figure 3 (a).

No irreversibility of the transient reflectivity was observed after exposing the sample to long trains of pump pulses at the highest  $F_P$  as shown in Figure 3b. To check for any heat build up effects single D-pulse experiments were also performed. No long-lived changes of the ultra-fast transient reflectivity were found.<sup>45</sup>

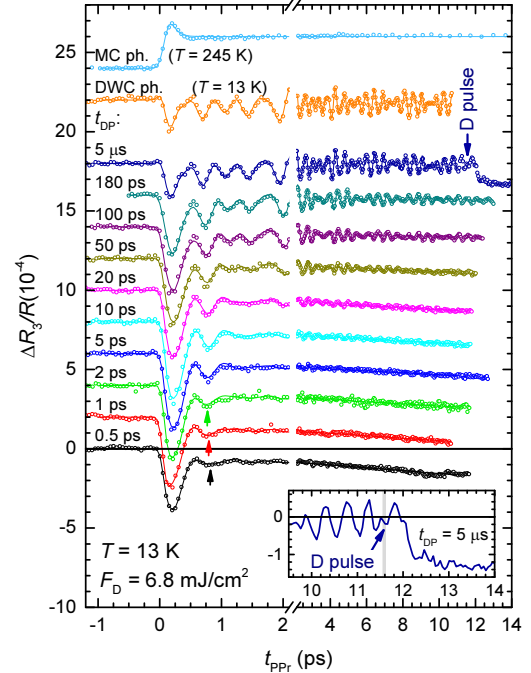


Figure 5. Multi-pulse transient reflectivity,  $\Delta R_3/R$ , as a function of the delay between the D and P pulses,  $t_{DP}$ . The arrows at the short- $t_{DP}$  scans emphasize the CO while the arrow at the  $t_{DP} = 5$ - $\mu$ s scan indicates the arrival of the subsequent D pulse. The two top-most traces, shown for comparison, correspond to the thermal equilibrium MC- and DWC-phase transient reflectivity. The traces are vertically offset for clarity and the thin lines in both panels correspond to the DECP model<sup>46</sup> fit (see SM<sup>45</sup>).

#### IV. DISCUSSION

The onset of the nonlinearities with increasing  $F_P$ , at  $F_{ce} \sim 0.6$  mJ/cm<sup>2</sup>, is mostly expressed in the SEC that can be associated with the electronic degrees of freedom only. The SEC total duration (including the risetime) of  $\sim 500$  fs significantly exceeds the time resolution of the setup ( $\sim 80$  fs) so the nonlinearity cannot be associated with the pump optical-transition nonlinearity, but is associated with the low-energy electronic degrees of freedom.

Focusing on the lattice degrees of freedom, which show strong  $F_P$  nonlinearity on the larger fluence scale above  $F_c$ , we first estimate the transient heating taking the  $T$ -dependent frequencies of the strongest two coherent modes,<sup>40</sup> O1 and O2 at 1.86 THz and 2.34 THz, respectively, as proxies for the lattice temperature. The obtained effective temperatures (see Figure 4 (d)) reach  $T_{IM}$  at a fluence that is close to  $F_c$ . This indicates that the symmetry-breaking lattice distortion is significantly affected only after the lattice degrees of freedom are heated close to  $T_{IM}$ . This is consistent with the absorbed energy at  $F_c$  that is comparable to the equilibrium enthalpy difference<sup>45</sup> between the high- $T$  MC phase at  $T \sim T_{IM}$

and the low- $T$  phase at  $T \sim 100$  K. Here the initial state  $T$  at  $t_{\text{DP}} \sim 5 \mu\text{s}$  (see Figure 6 (d)) is also estimated from the coherent mode frequencies.

The suppression of the CO with increasing  $F$  above  $F_c \sim 3 \text{ mJ}/\text{cm}^2$  is not abrupt as in the equilibrium case. This can be attributed to the finite-optical-penetration-depth induced excitation inhomogeneity. The thickens of a thin surface layer, within which the absorbed energy threshold is exceeded, reaches the optical penetration depth thickness only at the external fluence of  $e \times F_c \sim 8 \text{ mJ}/\text{cm}^2$ , consistent with the fluence where the CO are completely suppressed (see Figure 4 (c)). The excitation inhomogeneity results in a rather large error bar of  $F_c$ , of the order of  $\pm 0.5 \text{ mJ}/\text{cm}^2$ , but does not hinder a clear separation between  $F_{\text{ce}}$  and  $F_c$ .

The electronic ordering is therefore affected at lower excitation densities than the lattice order. The drop of  $\tau_e$  from the equilibrium value of a few picoseconds to  $\sim 200$  fs indicates that the gap-induced relaxation bottleneck<sup>40</sup> is transiently suppressed above  $F_{\text{ce}}$  already. The estimated photoexcited carriers density at  $F_{\text{ce}}$  is of the order<sup>45</sup> of  $10^{20} \text{ cm}^{-3}$  resulting in the plasma frequency of  $\sim 0.4 \text{ eV}$  that is larger than the insulating gap<sup>47</sup> of  $\Delta_I \sim 0.15 \text{ eV}$ . The bottleneck suppression can therefore be attributed to a sub-picosecond transient washout of the gap due to the (screening-induced) Mott transition that lasts at least few hundred fs. On this timescale a significant amount of the photoexcited carrier energy can be incoherently damped to phonons since the inelastic electron-phonon scattering time can be as fast as  $\sim 10$  fs<sup>48</sup>. However, the low frequency phonons corresponding to Ir-ions displacements<sup>40</sup> that set the lattice order parameter dynamics appear coherent until the gap is restored. According to Ref. [28] the equilibrium IM transition is a combination of orbital ordering and Peierls charge density wave transition. The Ir- $t_{2g}$ -orbitals derived bands are split (band Jahn-Teller effect) into two fully occupied  $xz$ - and  $yz$ -derived bands and a broader  $3/4$  occupied  $xy$ -derived band that simultaneously becomes gaped due to the Peierls tetramerization (see Fig 1 (c)). While the photoexcited Mott transition transiently suppresses the  $xy$ -derived band charge density wave, the band Jahn-Teller effect remains effective stabilizing the broken symmetry lattice deformation until the gap is restored. A similar decoupling of the electronic and lattice orders on a short timescale has been previously observed in  $\text{TiSe}_2$ .<sup>49</sup>

Turning to the highly excited transient state (HETS), the multi-pulse experiments clearly confirm that even at  $F_D \sim 8 \text{ mJ}/\text{cm}^2$  the excited volume does not switch into the high- $T$  MC state despite the large absorbed energy. In the most excited part of the volume, near the surface, the absorbed energy exceeds the equilibrium enthalpy difference between the high- $T$  MC state just above  $T_{\text{IM}}$  and the initial low- $T$  state by *more than two times*. The presence of the strongly damped broken-symmetry<sup>40</sup> CO with the unsuppressed initial amplitude (see Figure 6 (c)) indicates that the local lattice symmetry remains broken in

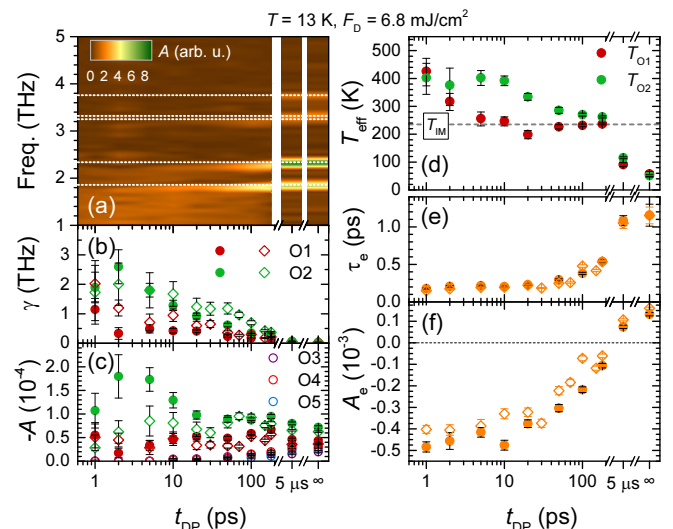


Figure 6. D-P delay dependence of the DECP fit parameters. (a) A density plot of the Fourier-transform spectra from data in Figure 5. The horizontal lines correspond to the equilibrium CO frequencies. (b) The CO dampings and (c) the corresponding amplitudes as a function of  $t_{\text{DP}}$ . (d) The effective temperature obtained from the frequency shifts of the two strongest coherent modes as a function of  $t_{\text{DP}}$ . (e) The relaxation time and (f) amplitude of the exponential components as a function of  $t_{\text{DP}}$ . Open diamonds in (b), (c), (e) and (f) correspond to the experiment at  $F_D = 8.1 \text{ mJ}/\text{cm}^2$ .

most of the excited volume, albeit with strong dephasing due to fluctuations and/or increased disorder.

The broken symmetry state could be stabilized by the pressure exerted by the surrounding unexcited bulk low- $T$  phase. Application of pressure is known to stabilize the triclinic insulating phase<sup>50</sup>, which has  $\sim 0.7$  % larger density<sup>51</sup> than the MC phase. Taking the compressibility<sup>52</sup>,  $\beta \sim 6 \cdot 10^{-3} \text{ GPa}^{-1}$ , one obtains the pressure of  $\sim 1.1 \text{ GPa}$  leading to an increase<sup>50</sup> of  $T_{\text{IM}}$  to  $T_{\text{IM}}' \sim 260 \text{ K}$ .

In addition to the  $T_{\text{IM}}$  increase, the pump optical penetration depth could increase due to the optical-transition bleaching at high- $F$  resulting in saturation of the absorbed energy density.<sup>42</sup> Such saturation cannot be entirely excluded and the maximum experimental  $T_{\text{eff}}$  indeed does not appear to significantly exceed  $T_{\text{IM}}'$  (Figures 4 (d) and 6 (d)). We should note, however, that at the high excitation  $T_{\text{eff}}$  does not directly correspond to the most excited volume region since the CO are inhomogeneously suppressed so  $T_{\text{eff}}$  is somewhat weighted towards the less-excited volume region.

While the above effects can contribute to stabilization of the broken symmetry state, they *cannot account* for the observed large CO dephasing. Extrapolating the equilibrium  $\gamma(T)$ <sup>40</sup> to the estimated<sup>45</sup> maximum possible transient  $T \sim 400 \text{ K}$  we obtain  $\gamma \sim 0.08$  and  $\sim 0.16$  for the O1 and O2 mode, respectively, which are at least  $\sim 5$  times smaller than the observed  $\gamma$  below  $t_{\text{DP}} \sim 20 \text{ ps}$  (Figure 6 (b)). The picosecond transient state there-

fore cannot be characterized as an ordinary super-heated equilibrium pressure-stabilized low- $T$  phase.

According to the classical kinetic theory of first order phase transitions<sup>53</sup> the formation of a stable phase from a metastable one proceeds through formation of macroscopic droplets that, due to the surface energy terms, grow deterministically only if their size exceeds a critical size,  $R_c$ . The nucleation of the droplets with  $R > R_c$  is a stochastic process driven either by fluctuations or tunneling, the later being proposed for the broken-symmetry-state droplet formation in the super-cooled early universe<sup>2</sup>. In the present case thermal fluctuations are likely large enough that the tunneling should not play any role.

The observed HETS could, therefore, be tentatively understood in this context where the fluctuating droplets of the high- $T$  MC phase introduce strong dynamical disorder into the triclinic phase matrix, but fail to reach the critical size or their growth is too slow to reach the MC phase before the heat diffusion spreads the absorbed energy across a larger volume, recovering the stability of the triclinic phase. Since there was no observable variation of the pump scattering with  $t_{DP}$  in the multipulse experiments the droplets are presumably much smaller than the pump wavelength of 800 nm and are most likely size-limited by the characteristic low- $T$ -phase twin lamella thickness<sup>54</sup> of  $\sim 20$  nm.

Increasing the excitation fluence beyond  $F \sim 8$  mJ/cm<sup>2</sup> the standard 2-pulse  $\Delta R/R$  (see Fig. 3 (c)) shows evolution of a broad dip between  $\sim 10$  and  $\sim 200$  ps. The dip might signify an onset of MC-phase droplets growth. Unfortunately, this excitation region was not investigated in multipulse experiments in order to avoid sample cracking<sup>55</sup> due to the high D-beam average thermal load<sup>56</sup>. Further experiments with lower repetition laser source are therefore necessary to reach a more definitive conclusion regarding the behavior beyond  $F \sim 8$  mJ/cm<sup>2</sup>.

The HETS is expected to be quite metallic and different from the DWC state since the sub-picosecond component behavior indicates the suppression of the gap at lower  $F$  already. However, the evidence is indirect so more direct experimental evidence from time-resolved low-energy probes is necessary to clearly establish the degree of metallicity.

Since the HETS state appears after strong ultrafast excitation on a sub-picosecond timescale, in a manner similar to the metastable metallic H phase<sup>11,57</sup> in  $1T$ -TaS<sub>2</sub>, it is necessary to compare the phenomena.  $1T$ -TaS<sub>2</sub> is, unlike CuIr<sub>2</sub>S<sub>4</sub>, a layered compound with the equilibrium phase diagram that is significantly more complicated than the phase diagram of CuIr<sub>2</sub>S<sub>4</sub>. In particular, the low- $T$  insulating commensurate (C) polaron ordered phase is separated from the symmetric high- $T$  metallic phase ( $T > 543$  K) by intermediate incommensurate polaron ordered phases that are quite conducting.

The H phase is created after the C phase exposure to a single ultrafast optical pulse above a critical fluence,

$F_H \sim 1$  mJ/cm<sup>2</sup>.<sup>11</sup> On the long timescales the H phase appears as a disordered texture of the frozen C-phase polaron domains<sup>58</sup>. An additional metastable amorphous (A) polaron glass phase has also been observed recently that is created at higher excitation fluences than the H phase,  $F \gtrsim F_A \sim 3.5$  mJ/cm<sup>2</sup>.<sup>59</sup>

The spatial textures of the H and A phases and their evolution on the ultrafast timescales have not been yet determined and the microscopic pathway from the C to either H or A phase is still unclear. Since different C-phase domains in the H phase have different phase shifts relative to the underlying atomic lattice<sup>58</sup> a global reconfiguration of the polaron lattice must take place during the transition already above  $F_H$ . This implies that the C polaron lattice “melts” into some transient state before condensing into the H (A) phase. This transient state could be, similarly to the present case on the picoseconds timescales, composed from droplets of a “melted” phase that are embedded into the C phase. The droplet phase could correspond to either some incommensurate phase, polaron liquid or even the high- $T$  metallic phase without polarons.

The CO in  $1T$ -TaS<sub>2</sub> are not so strongly suppressed during the creation of the H phase and become suppressed only for  $F > F_A$ .<sup>60,61</sup> The H phase creation conditions in  $1T$ -TaS<sub>2</sub> are therefore more similar to the excitation above  $F_{ce}$  in CuIr<sub>2</sub>S<sub>4</sub>, where the lattice  $T$  remains below  $T_{IM}$ , while the fluences above  $F_c$ , where also the lattice  $T$  transiently exceeds  $T_{IM}$ , correspond better to the A-phase creation conditions in  $1T$ -TaS<sub>2</sub>. Owing to the similar penetration depths of  $\sim 30$  nm and  $\sim 40$  nm in  $1T$ -TaS<sub>2</sub><sup>59</sup> and CuIr<sub>2</sub>S<sub>4</sub><sup>45</sup>, respectively, and the similar equilibrium transition temperatures it is not surprising that  $F_c$  and  $F_A$  are rather similar.

Contrary to  $1T$ -TaS<sub>2</sub> in CuIr<sub>2</sub>S<sub>4</sub> the same DWC state forms on the long timescales irrespective of the excitation fluence and the excitation type. It was shown<sup>37,39</sup> that in the DWC state the long range low- $T$  order is replaced by a short range ( $\xi \sim 2$  nm) incommensurate modulation with preserved *local* Ir<sup>4+</sup> dimerization. The DWC state is, therefore, structurally more comparable to the A phase than the H phase of  $1T$ -TaS<sub>2</sub>. However, the electronic gap in the DWC state is not suppressed<sup>38</sup> like in the A state of  $1T$ -TaS<sub>2</sub><sup>59</sup> and the resistivity is larger,  $\rho \sim 65$   $\Omega$ cm, than in the A state of  $1T$ -TaS<sub>2</sub> with  $\rho$  in the  $\sim 10$  m $\Omega$  range<sup>59</sup>. The DWC and A state (as well as H state) are therefore quite different. This could be connected to the absence of strong correlations and weak neighboring Ir-ion chain coupling in CuIr<sub>2</sub>S<sub>4</sub> making the electronic gap less sensitive to the disorder-induced doping.

Comparing CuIr<sub>2</sub>S<sub>4</sub> with VO<sub>2</sub> and V<sub>2</sub>O<sub>3</sub> we observe similarities, but also differences. All three compounds show transient intermediate states with suppressed gaps<sup>12,13,18,21</sup> that are structurally distinct from the high- $T$  metallic phases suggesting a transient decoupling of the structural and electronic orders. The decoupling in both oxides has been attributed to the correla-

tion effects<sup>13,18</sup>. In our case, however, the effect can be attributed to a photoinduced Mott transition.

The timescales of the structural transitions are quite different. In VO<sub>2</sub> the transition is abrupt<sup>19,24,25</sup> while V<sub>2</sub>O<sub>3</sub><sup>21,23</sup> and CuIr<sub>2</sub>S<sub>4</sub> show first-order kinetics bottlenecks which slow down the transition. In this context it is worth noting that the lattice volume change at the equilibrium IM transition is the smallest, 0.1 % in VO<sub>2</sub><sup>62</sup> in comparison to -1.3 % in V<sub>2</sub>O<sub>3</sub><sup>63</sup> and 0.7 % in CuIr<sub>2</sub>S<sub>4</sub><sup>51</sup>, suggesting a smaller inter-phase-boundary energy cost enabling easier nucleation of the high-*T* metallic phase droplets.

## V. CONCLUSIONS

We showed that in the strongly nonequilibrium regime upon a femtosecond photoexcitation the low-temperature ultrafast structural dynamics in CuIr<sub>2</sub>S<sub>4</sub> is dominated by the first-order-transition nucleation kinetics that prevents the complete ultrafast photoinduced structural transition into the high-*T* phase at unexpectedly large

excitation densities. Concurrently, the dynamically-decoupled electronic order is suppressed rather independently on a sub-picosecond timescale at much weaker excitation density. While the electronic order suppression likely results in a transient metallization of the highly nonequilibrium broken lattice-symmetry state no evidence was found that femtosecond excitation would lead to a long lived metastable state more conducting than the slowly formed disordered weakly conducting phase.

## ACKNOWLEDGMENTS

The authors acknowledge the financial support of Slovenian Research Agency (research core funding No-P1-0040 and young researcher funding No. 50504) for financial support. We would also like to thank V. Nasretinova and E. Goreschnik for the help at the sample characterization, M. Aničin and A. Bavec for help at transient reflectivity measurements and E. Bozin for fruitful discussions.

- 
- \* \* tomaz.mertelj@ijs.si
- <sup>1</sup> P. Papon, J. Leblond, and P. H. Meijer, *Physics of Phase Transitions* (Springer, 2002).
  - <sup>2</sup> A. D. Linde, *Physics Letters B* **108**, 389 (1982).
  - <sup>3</sup> M. F. Becker, A. B. Buckman, R. M. Walser, T. Lépine, P. Georges, and A. Brun, *Applied Physics Letters* **65**, 1507 (1994).
  - <sup>4</sup> M. Fiebig, K. Miyano, Y. Tomioka, and Y. Tokura, *Journal of Luminescence* **87**, 82 (2000).
  - <sup>5</sup> A. Cavalleri, C. Tóth, C. W. Siders, J. Squier, F. Ráksi, P. Forget, and J. Kieffer, *Physical review letters* **87**, 237401 (2001).
  - <sup>6</sup> L. Perfetti, P. Loukakos, M. Lisowski, U. Bovensiepen, H. Berger, S. Biermann, P. Cornaglia, A. Georges, and M. Wolf, *Physical review letters* **97**, 067402 (2006).
  - <sup>7</sup> P. Baum, D.-S. Yang, and A. H. Zewail, *Science* **318**, 788 (2007), <https://science.sciencemag.org/content/318/5851/788.full.pdf>.
  - <sup>8</sup> S. Wall, D. Wegkamp, L. Foglia, K. Appavoo, J. Nag, R. Haglund, J. Stähler, and M. Wolf, *Nature communications* **3**, 1 (2012).
  - <sup>9</sup> S. De Jong, R. Kukreja, C. Trabant, N. Pontius, C. Chang, T. Kachel, M. Beye, F. Sorgenfrei, C. Back, B. Bräuer, *et al.*, *Nature materials* **12**, 882 (2013).
  - <sup>10</sup> N. Fukazawa, T. Tanaka, T. Ishikawa, Y. Okimoto, S.-y. Koshihara, T. Yamamoto, M. Tamura, R. Kato, and K. Onda, *The Journal of Physical Chemistry C* **117**, 13187 (2013).
  - <sup>11</sup> L. Stojchevska, I. Vaskivskiy, T. Mertelj, P. Kusar, D. Svetin, S. Brazovskii, and D. Mihailovic, *Science* **344**, 177 (2014).
  - <sup>12</sup> V. R. Morrison, R. P. Chatelain, K. L. Tiwari, A. Hendaoui, A. Bruhács, M. Chaker, and B. J. Siwick, *Science* **346**, 445 (2014).
  - <sup>13</sup> D. Wegkamp, M. Herzog, L. Xian, M. Gatti, P. Cudazzo, C. L. McGahan, R. E. Marvel, R. F. Haglund Jr, A. Rubio, M. Wolf, *et al.*, *Physical review letters* **113**, 216401 (2014).
  - <sup>14</sup> E. Abreu, S. Wang, J. G. Ramírez, M. Liu, J. Zhang, K. Geng, I. K. Schuller, and R. D. Averitt, *Physical Review B* **92**, 085130 (2015).
  - <sup>15</sup> B. T. O’Callahan, A. C. Jones, J. H. Park, D. H. Cobden, J. M. Atkin, and M. B. Raschke, *Nature communications* **6**, 1 (2015).
  - <sup>16</sup> K. Haupt, M. Eichberger, N. Erasmus, A. Rohwer, J. Demsar, K. Rossnagel, and H. Schwoerer, *Physical review letters* **116**, 016402 (2016).
  - <sup>17</sup> J. Zhang, X. Tan, M. Liu, S. W. Teitelbaum, K. W. Post, F. Jin, K. A. Nelson, D. Basov, W. Wu, and R. D. Averitt, *Nature materials* **15**, 956 (2016).
  - <sup>18</sup> G. Lantz, B. Mansart, D. Grieger, D. Boschetto, N. Nilforoushan, E. Papalazarou, N. Moisan, L. Perfetti, V. L. Jacques, D. Le Bolloc’h, *et al.*, *Nature communications* **8**, 1 (2017).
  - <sup>19</sup> M. F. Jager, C. Ott, P. M. Kraus, C. J. Kaplan, W. Pouse, R. E. Marvel, R. F. Haglund, D. M. Neumark, and S. R. Leone, *Proceedings of the National Academy of Sciences* **114**, 9558 (2017).
  - <sup>20</sup> C. Laulhé, T. Huber, G. Lantz, A. Ferrer, S. O. Mariager, S. Grübel, J. Rittmann, J. A. Johnson, V. Esposito, A. Lübcke, *et al.*, *Physical review letters* **118**, 247401 (2017).
  - <sup>21</sup> A. Singer, J. G. Ramirez, I. Valmianski, D. Cela, N. Hua, R. Kukreja, J. Wingert, O. Kovalchuk, J. M. Glownia, M. Sikorski, *et al.*, *Physical review letters* **120**, 207601 (2018).
  - <sup>22</sup> M. Ligges, I. Avigo, D. Golež, H. Strand, Y. Beyazit, K. Hanff, F. Diekmann, L. Stojchevska, M. Kalläne, P. Zhou, *et al.*, *Physical review letters* **120**, 166401 (2018).

- <sup>23</sup> A. Ronchi, P. Homm, M. Menghini, P. Franceschini, F. Maccherozzi, F. Banfi, G. Ferrini, F. Cilento, F. Parmigiani, S. Dhesi, *et al.*, *Physical Review B* **100**, 075111 (2019).
- <sup>24</sup> S. Wall, S. Yang, L. Vidas, M. Chollet, J. M. Glowia, M. Kozina, T. Katayama, T. Henighan, M. Jiang, T. A. Miller, D. A. Reis, L. A. Boatner, O. Delaire, and M. Trigo, *Science* **362**, 572 (2018), <https://science.sciencemag.org/content/362/6414/572.full.pdf>.
- <sup>25</sup> M. R. Otto, L. P. René de Cotret, D. A. Valverde-Chavez, K. L. Tiwari, N. Émond, M. Chaker, D. G. Cooke, and B. J. Siwick, *Proceedings of the National Academy of Sciences* **116**, 450 (2019), <https://www.pnas.org/content/116/2/450.full.pdf>.
- <sup>26</sup> L. Vidas, D. Schick, E. Martínez, D. Perez-Salinas, A. Ramos-Álvarez, S. Cichy, S. Batlle-Porro, A. S. Johnson, K. A. Hallman, R. F. Haglund Jr, *et al.*, *Physical Review X* **10**, 031047 (2020).
- <sup>27</sup> K. Momma and F. Izumi, *Journal of applied crystallography* **44**, 1272 (2011).
- <sup>28</sup> D. Khomskii and T. Mizokawa, *Physical review letters* **94**, 156402 (2005).
- <sup>29</sup> S. Sarkar, M. De Raychaudhury, and T. Saha-Dasgupta, *Physical Review B* **79**, 113104 (2009).
- <sup>30</sup> S. Nagata, T. Hagino, Y. Seki, and T. Bitoh, *Physica B: Condensed Matter* **194**, 1077 (1994).
- <sup>31</sup> H. Ishibashi, T. Sakai, and K. Nakahigashi, *Journal of magnetism and magnetic materials* **226**, 233 (2001).
- <sup>32</sup> P. G. Radaelli, Y. Horibe, M. J. Gutmann, H. Ishibashi, C. Chen, R. M. Ibberson, Y. Koyama, Y.-S. Hor, V. Kiryukhin, and S.-W. Cheong, *Nature* **416**, 155 (2002).
- <sup>33</sup> T. Sasaki, M. Arai, T. Furubayashi, and T. Matsumoto, *Journal of the Physical Society of Japan* **73**, 1875 (2004).
- <sup>34</sup> H. Ishibashi, T. Koo, Y. S. Hor, A. Borisso, P. G. Radaelli, Y. Horibe, S. Cheong, and V. Kiryukhin, *Physical Review B* **66**, 144424 (2002).
- <sup>35</sup> T. Furubayashi, H. Suzuki, T. Matsumoto, and S. Nagata, *Solid state communications* **126**, 617 (2003).
- <sup>36</sup> K. Takubo, S. Hirata, J.-Y. Son, J. Quilty, T. Mizokawa, N. Matsumoto, and S. Nagata, *Physical review letters* **95**, 246401 (2005).
- <sup>37</sup> V. Kiryukhin, Y. Horibe, Y. S. Hor, H. Noh, S. Cheong, and C. Chen, *Physical review letters* **97**, 225503 (2006).
- <sup>38</sup> K. Takubo, T. Mizokawa, N. Matsumoto, and S. Nagata, *Physical Review B* **78**, 245117 (2008).
- <sup>39</sup> E. Božin, A. S. Masadeh, Y. S. Hor, J. Mitchell, and S. Billinge, *Physical review letters* **106**, 045501 (2011).
- <sup>40</sup> M. Naseska, P. Sutar, D. Vengust, S. Tsuchiya, M. Čeh, D. Mihailovic, and T. Mertelj, *Physical Review B* **101**, 165134 (2020).
- <sup>41</sup> R. Yusupov, T. Mertelj, V. V. Kabanov, S. Brazovskii, P. Kusar, J.-H. Chu, I. R. Fisher, and D. Mihailovic, *Nature Physics* **6**, 681 (2010).
- <sup>42</sup> M. Naseska, A. Pogrebna, G. Cao, Z. Xu, D. Mihailovic, and T. Mertelj, *Physical Review B* **98**, 035148 (2018).
- <sup>43</sup> I. Madan, V. Baranov, Y. Toda, M. Oda, T. Kurosawa, V. Kabanov, T. Mertelj, and D. Mihailovic, *Physical Review B* **96**, 184522 (2017).
- <sup>44</sup> M. Koshimizu, H. Tsukahara, and K. Asai, *Nuclear Instruments and Methods in Physics Research Section B: Beam Interactions with Materials and Atoms* **267**, 1125 (2009).
- <sup>45</sup> M. Naseska, P. Sutar, D. Vengust, D. Svetin, Y. Vaskivskiy, I. Vaskivskiy, D. Mihailovic, and T. Mertelj, (2021), supplemental Material.
- <sup>46</sup> H. Zeiger, J. Vidal, T. Cheng, E. Ippen, G. Dresselhaus, and M. Dresselhaus, *Physical Review B* **45**, 768 (1992).
- <sup>47</sup> N. Wang, G. Cao, P. Zheng, G. Li, Z. Fang, T. Xiang, H. Kitazawa, and T. Matsumoto, *Physical Review B* **69**, 153104 (2004).
- <sup>48</sup> M. Lundstrom, “Carrier scattering,” in *Fundamentals of Carrier Transport* (Cambridge University Press, 2000) pp. 54–118, 2nd ed.
- <sup>49</sup> M. Porer, U. Leierseder, J.-M. Ménard, H. Dachraoui, L. Mouchliadis, I. Perakis, U. Heinzmann, J. Demsar, K. Rossnagel, and R. Huber, *Nature materials* **13**, 857 (2014).
- <sup>50</sup> G. Oomi, T. Kagayama, I. Yoshida, T. Hagino, and S. Nagata, *Journal of magnetism and magnetic materials* **140**, 157 (1995).
- <sup>51</sup> T. Furubayashi, T. Matsumoto, T. Hagino, and S. Nagata, *Journal of the Physical Society of Japan* **63**, 3333 (1994).
- <sup>52</sup> A. B. Garg, V. Vijayakumar, B. K. Godwal, A. Choudhury, and H. D. Hochheimer, *Solid state communications* **142**, 369 (2007).
- <sup>53</sup> E. Lifshitz, L. Pitaevskii, J. Sykes, and R. Franklin, *Physical Kinetics: Volume 10*, Course of theoretical physics (Elsevier Science, 1995).
- <sup>54</sup> W. Sun, T. Kimoto, T. Furubayashi, T. Matsumoto, S. Ikeda, and S. Nagata, *Journal of the Physical Society of Japan* **70**, 2817 (2001).
- <sup>55</sup> Observed in earlier experiments upon high laser induced average thermal load.
- <sup>56</sup> The average thermal load in the multipulse experiments is doubled with respect to the standard 2-pulse experiments since D-beam is unchopped.
- <sup>57</sup> J. Ravnik, *Studies of ultrafast processes in correlated materials using scanning tunnelling microscope*, Ph.D. thesis, Univerza v Ljubljani, Fakulteta za matematiko in fiziko (2019).
- <sup>58</sup> Y. A. Gerasimenko, P. Karpov, I. Vaskivskiy, S. Brazovskii, and D. Mihailovic, *npj Quantum Materials* **4**, 1 (2019).
- <sup>59</sup> Y. A. Gerasimenko, I. Vaskivskiy, M. Litskevich, J. Ravnik, J. Vodeb, M. Diego, V. Kabanov, and D. Mihailovic, *Nature materials* **18**, 1078 (2019).
- <sup>60</sup> J. Ravnik, I. Vaskivskiy, T. Mertelj, and D. Mihailovic, *Physical Review B* **97**, 075304 (2018).
- <sup>61</sup> J. Ravnik, M. Diego, Y. Gerasimenko, Y. Vaskivskiy, I. Vaskivskiy, T. Mertelj, J. Vodeb, and D. Mihailovic, arXiv preprint arXiv:2011.00930 (2020).
- <sup>62</sup> M. Marezio, P. Dernier, D. McWhan, and J. Remeika, *Materials Research Bulletin* **5**, 1015 (1970).
- <sup>63</sup> P. Rozier, A. Ratuszna, and J. Galy, *Zeitschrift für anorganische und allgemeine Chemie* **628**, 1236 (2002).